

Rolf F. Hertenstein<sup>1</sup> and Joachim Kuettner<sup>2</sup><sup>1</sup>Colorado Research Associates division of NWRA, Boulder, Colorado<sup>2</sup>UCAR, Boulder, Colorado

## 1. INTRODUCTION

The observations discussed by Kuettner and Hertenstein (2002) suggest that two types of rotor exist. Type 1 rotors have associated moderate and sometimes severe turbulence as encountered by pilots transitioning this type of rotor. Tops of rotor turbulence are usually comparable to those of the upstream inversion over the mountain range. Type 2 rotors, by contrast, reach heights far exceeding the upstream inversion. They have certain characteristics of a hydraulic jump and always contain severe, and sometimes extreme turbulence, presenting an extraordinary hazard to aviation.

To further understand the dynamics and evolution of rotors, high-resolution, two-dimensional simulations were performed. We have tried to reproduce the two types of rotor, and determine the conditions under which they form. We have also sought criteria which may allow us to distinguish cases in which rotors appear to be induced by mountain waves from those in which the opposite appears to take place. In exploring these issues we have varied the initial wind profiles in order to represent actual upstream soundings observed during the Sierra Wave Project (SWP).

Finally, we have run sensitivities to determine the effect of several related phenomena observed during the SWP. These include the effects of surface heating, moisture, and the presence of a second mountain range (e.g., the Inyo Mountains downstream of the Sierra Nevada).

## 2. INVESTIGATIVE PROCEDURE

The mesoscale model used was the Regional Atmospheric Modeling System, (RAMS, Pielke et al. 1992). Horizontal grid spacing of 150 m was employed over 1700 points. Vertical spacing was 20 m at the lowest level then stretched to a maximum of 150 m over 145 points with a sponge layer at the upper boundary. No-slip lower boundary conditions were used. A 2500 m skewed Witch of Agnese mountain was employed with a 40 km half width on the upstream side and 5 km half width on the lee side. Runs presented here did not use a soil model or radiation parameterization (i.e., no heat transfer from the surface) and were run with no moisture. Runs including heat and moisture will be presented at the conference. Quasi steady state was usually achieved within 3 h simulation time.

In exploring the different types of rotors, we varied

the upstream wind and temperature profiles to reflect the often observed inversions and peaked vs. blunt jet-stream profiles. The initial soundings for our runs were reconstructed from available data sources for several days during the SWP. The temperature profile was the same for each run presented here. The lowest level (surface to 200 m above mountain top) features a potential temperature ( $\theta$ ) gradient of  $7.4 \times 10^{-4} \text{ K km}^{-1}$ . This is capped by a 600 m deep, 10 K inversion. Between the inversion top and the tropopause,  $\theta$  increases by  $3 \times 10^{-3} \text{ K km}^{-1}$ . Wind profiles vary and are described for each run in the section below.

## 3. RESULTS

Figure 1 shows  $\theta$  for a 100 km portion of the domain for RUN1 and  $t = 3 \text{ h}$ , at which time the flow is quasi-steady. The model was initialized with winds increasing linearly at  $4.2 \times 10^{-3} \text{ s}^{-1}$  to a maximum of  $50 \text{ ms}^{-1}$  at the 10.5 km tropopause, with a decrease of  $4.9 \times 10^{-3} \text{ s}^{-1}$  in the stratosphere.

The flow field resembles a hydraulic jump, with a vertically-propagating primary wave, and turbulent flow extending more than 60 km downstream. There is some agreement between the simulated flow and the conceptual model derived from experience in the SWP (Kuettner, 1959, see his Fig. 8). Vertical velocity ( $w$ ) in the primary updraft in the laminar flow is almost  $20 \text{ ms}^{-1}$ , while rotor updrafts and downdrafts are  $O(\pm 12 \text{ ms}^{-1})$ . Lee downslope winds reach a maximum of  $52 \text{ ms}^{-1}$  near the base of the lee slope. Note that an extended region of breaking occurs in the stratosphere at  $z = 15 \text{ km}$ .

Figure 2 shows streamlines for RUN1 for a 15 km portion of the domain centered on the jump and rotor directly under it. The Type 2 rotor is apparent. Turbulent eddies, with horizontal vorticity ( $\eta$ ) of both signs are seen to extend well above the upstream inversion (see also Fig. 1). The rotor flow leads to strong horizontal shear in  $w$ , e.g.,  $18 \text{ ms}^{-1}$  over a horizontal distance of 1 km. As noted by Kuettner and Hertenstein (2002), shears an order of magnitude stronger than those simulated here were observed by aircraft during the SWP.

The next experiment (RUN2) uses the same linear wind shear above and below the inversion as in RUN1. However, the initial flow increases  $8 \text{ ms}^{-1}$  through the 600 m inversion leading to a maximum tropopause wind of  $58 \text{ ms}^{-1}$ .

Figure 3 shows  $\theta$  for a 100 km portion of the domain for RUN2 and  $t = 3 \text{ h}$  (cf. Fig. 1). The mountain wave is partially trapped; some energy is seen to 'leak' upwards and perturb the stratosphere. Downslope winds along the lee slope are about  $10 \text{ ms}^{-1}$  weaker than RUN1.

---

\* Corresponding author address: Rolf F. Hertenstein, Colorado Research Associates, a division of NWRA,, 3380 Mitchell Lane, Boulder, CO 80301, herten@co-ra.com

Streamlines (Fig. 4) show that Type 1 rotors have formed, with  $\eta$  of similar sign to trapped waves simulated by Doyle and Durran (2002). In our simulation, two distinct rotors have formed under the first wave crest.

The counter-rotating ( $-\eta$ ) eddies simulated in RUN1 do not fit conventional conceptual models of rotor flow. In order to better understand the evolution of the Type 2 rotor, RUN1 was repeated with model topography 1500 m higher to make direct comparisons with SWP observations easier. The peak to valley drop is still 2500m. Model output was inspected at every 2 minutes of simulation time. We found that events in the first 15 minutes of the simulation largely determine the flow field in the remainder of the simulation. After only 2 min,  $u$  at the mountain crest has already increased from 16 to 24  $\text{ms}^{-1}$  and continues to accelerate down the lee slope over the next several minutes. By 14 min,  $\eta$  reaches  $0.1 \text{ s}^{-1}$  in near-surface shear, with  $-0.04 \text{ s}^{-1}$  above the 'shooting' downslope flow, which is confined to a layer only 200-300 m above the surface. Convergence at the head of the shooting flow leads to  $w = 9 \text{ ms}^{-1}$ , which steepens  $\theta$  to the point that breaking has begun, as determined by vertical isentropes. The strong updraft has also transported  $\eta$  of both signs upwards (Fig. 5). By this time,  $-\eta$  has reached 4 km and is being advected westward by 2  $\text{ms}^{-1}$  easterly  $u$  at that level, thus producing a counter-rotating ( $-\eta$ ) rotor. The evolution up to this time resembles that simulated by Rotunno and Smolarkiewicz (1995, see their Fig. 3). At this point it is clear that a primary rotor has established itself before deeply vertically-propagating waves have formed above.

Over the next 30 min, turbulent flow beneath the jump intensifies and propagates downstream. Above the jump, the vertically-propagating wave intensifies, while a primary wavelength of 20 km establishes itself. Time lapse of the modeled flow shows that the lower part of the mountain wave is frequently perturbed by coherent eddies ( $O(4 \text{ km})$  in diameter) which form along the leading edge of the primary rotor and are then advected upwards and downstream. Several coherent eddies exist within what might be better referred to as a rotor zone. In addition, perturbations sometimes occur further downstream in the rotor zone, which at times leads to a deeper rotor zone downstream of the primary wave.

Further simulations were run to investigate the sensitivity of RUN1 and RUN2 to details in the wind and stability profile. Analysis of these simulations is currently underway; results will be reported at the conference.

A simulation was run in which the model topography was modified to add a second mountain range resembling the Inyo Mountains east of the Sierra Nevada. The initial sounding was the same as RUN1. Figure 6 shows  $\theta$  for a 100 km portion of the domain at  $t = 3 \text{ h}$  (cf. Fig. 1). The response due to the addition of the Inyos is dramatic. The Inyos appear to influence the low-level shooting flow, so that the very steep jump occurs 5-6 km closer to the upstream mountain. One large rotor, with positive  $\eta$  occurs in the well-mixed region centered on  $x = 25 \text{ km}$  and  $z = 4000 \text{ m}$ . Maximum rotor height is

reduced compared to RUN1 (by approximately 1500 m), as are maximum values of  $\eta$  (from  $0.077$  to  $0.045 \text{ s}^{-1}$ ) on the leading edge of the rotor. As opposed to strong westerly flow under the primary rotor of RUN1, the addition of the Inyos leads to easterly surface flow. Lastly, the addition of the Inyos has modified the character and horizontal extent of the wave breaking in the stratosphere.

#### 4. PRELIMINARY CONCLUSIONS

We have simulated flow over steep lee-slope topography to better understand the rotor dynamics associated with the more powerful Type 2 rotor compared to the Type1 rotor. Preliminary results are as follows:

1. Type 1 rotors seem to form preferably with trapped waves, while Type 2 rotors form with vertically-propagating waves.

2. Type 2 rotors display internal circulations with enormous vertical motions exceeding  $\pm 20 \text{ ms}^{-1}$  and horizontal vorticity of  $O(0.1 \text{ s}^{-1})$ .

3. Stratospheric wave breaking occurred with each simulation. Analysis is currently underway to better understand this response.

4. We have encountered difficulties in determining which wind and temperature profile clearly produces trapped vs. vertically-propagating waves in the presence of rotors. This work is currently underway.

#### 5. REFERENCES

- Doyle, J.D., and D.R. Durran, 2002: The dynamics of mountain-wave-induced rotors. *J. Atmos. Sci.*, **59**, 186-201.
- Kuettnner, J., 1959: The rotor flow in the lee of mountains. GRD Research Notes No. 6, Air Force Cambridge Research Center, 20 pp.
- Kuettnner, J. and R.F. Hertenstein, 2002: Observations of mountain-wave-induced rotors and related hypotheses: A review. *Preprints, Tenth Conference on Mountain Meteorology*. 17-21 June 2002, Park City, UT. (This volume).
- Pielke, R.A., W.R. Cotton, R.L. Walko, C.J. Tremback, W.A. Lyons, L.D. Grasso, M.E. Nicholls, M.D. Moran, D.A. Wesley, T.J. Lee, and J.H. Copeland, 1992: A comprehensive meteorological modeling system - RAMS. *Meteor. Atmos. Phys.*, **49**, 69-91.
- Rotunno, R. and P.K. Smolarkiewicz, 1995: Vorticity generation in the shallow-water equations as applied to hydraulic jumps. *J. Atmos. Sci.*, **52**, 320-330.

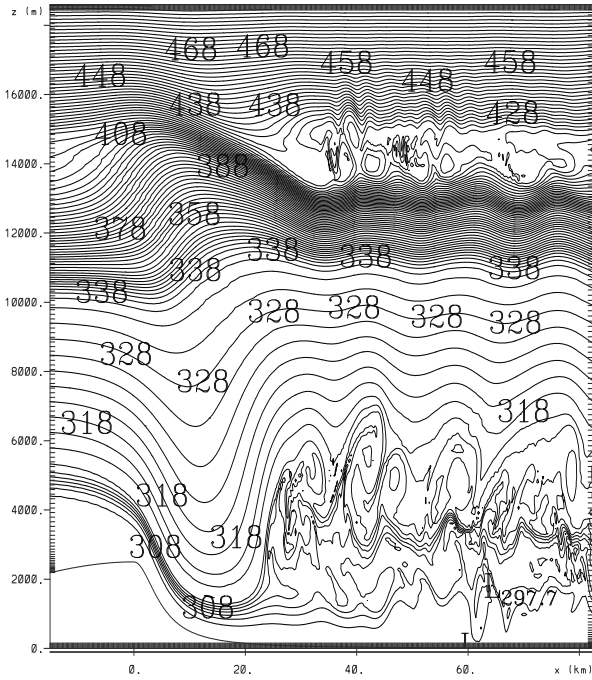


Figure 1. Potential temperature for RUN1 at 3 h. Contour interval is 2 K. Note the wave breaking region above the tropopause.

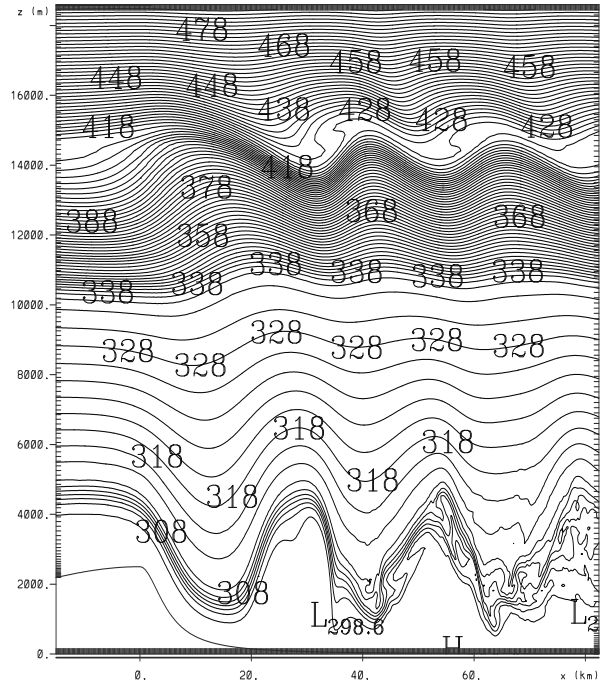


Figure 3. As Fig. 1 except for RUN2.

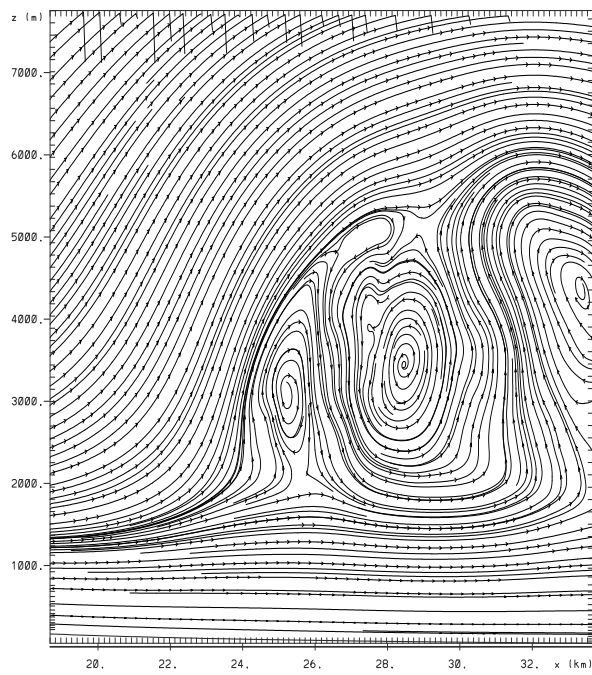


Figure 2. Streamlines for RUN1 at 3 h.

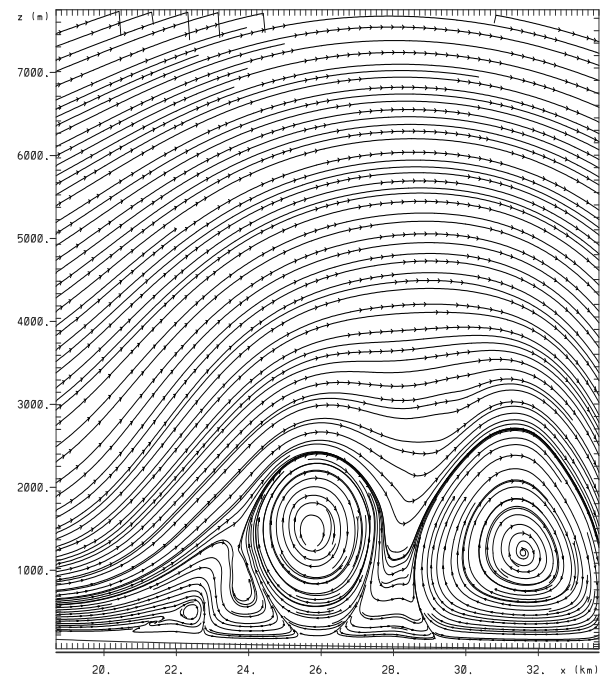


Figure 4. Streamlines for RUN2 at 3 h.

